DOI: 10.1002/ejic.200701350

Electron-Sponge Behavior, Reactivity and Electronic Structures of Cobalt-Centered Cubic $Co_9Te_6(CO)_8$ Clusters

Mustapha Bencharif,[a] Olivier Cador,[b] Hélène Cattey,[c] Alexander Ebner,[d] Jean-François Halet,[b] Samia Kahlal,[b] Walter Meier,[d] Yves Mugnier,[c] Jean-Yves Saillard,[b] Patrick Schwarz,[d] Fatima Zohra Trodi,[a,b] Joachim Wachter,*[d] and Manfred Zabel[d]

Keywords: Cobalt / Tellurium / Cluster / Electrochemistry / Electronic structure

Extended investigations of the reaction sequence $[Cp'_2Nb(Te_2)H]/CH_3Li/[Co_2(CO)_8]$ ($Cp' = tBuC_5H_4$) led to the identification of $Li_n[\mathbf{3}]$ {$\mathbf{3} = [Co_9Te_6(CO)_8]$; $n = 1, 2$} salts through their transformation with [PPN]Cl into $[PPN]_n[\mathbf{3}]$ ($PPN = Ph_3PNPPh_3$). These compounds form in the solid state columnar ([PPN][**3**]) or undulated 2D ($[PPN]_2[\mathbf{3}]$) supramolecular networks. Electrochemical studies of $[Cp^*_2Nb(CO)_2][\mathbf{3}]$ ($Cp^* = C_5Me_5$) or $[Na(THF)_6][\mathbf{3}]$ revealed the presence of the redox couples $[\mathbf{3}]^-/[\mathbf{3}]^{2-}/[\mathbf{3}]^{3-}/[\mathbf{3}]^{4-}/[\mathbf{3}]^{5-}$ regardless of the nature of the cation, whereas in the anodic part oxidative degradation of the cluster takes place. This behavior is in agreement with the observation that $[\mathbf{3}]^-$ containing salts form with PPh_3AuCl or dppe decomposition products like $[(PPh_3)_2Au][CoCl_3PPh_3]$ or $[Co(CO)_2dppe]_2(\mu\text{-Te})$. A neutral cluster comprising the $Co@Co_8(\mu_4\text{-Te})_6$ core formed in the reaction of $[Cp^*_2Nb(CO)_2][Co_{11}Te_7(CO)_{10}]$ with PPh_3AuCl, which gave $[Co_9Te_6(CO)_4(PPh_3)_4]$ (**4**) after oxidative cluster degradation and CO substitution. **4** was characterized by X-ray crystallography. DFT calculations carried out on all members of the $[\mathbf{3}]^n$ ($n = +1$ to -5) family and on related species indicate that there is no significant Jahn–Teller distortion (and therefore no connectivity change) for any of the considered electron counts. Magnetic investigations on [PPN][**3**] show that the ground state of $[\mathbf{3}]^-$ is a spin triplet with spins interacting antiferromagnetically in a 1D space.

Introduction

Hexacapped cubic transition metal clusters cover a wide range of electron counts.[1] Only a limited set of metals (M = Ni, Pd) and ligands (E = GeEt, As, Te) is available for metal-centered hexacapped $M_9(\mu_4\text{-E})_6L_8$ clusters.[2] In these clusters 120 to 130 metal valence electron (MVE) counts are observed. Only little is known on their reactivity except that some of these compounds exhibit at least three stable reversible or quasi-reversible redox systems.[3] An important prerequisite for electron-sponge behavior in transition-metal clusters is associated to the lack of any significant Jahn–Teller instability for a range of electron counts, the upper limit of which being generally that which satisfies the closed-shell principle.[1c,1d] Whereas thermal stability generally arises when the closed-shell principle is satisfied, this is most often not the case in molecular compounds for lower electron counts for which first- or second-order Jahn–Teller distortions are anticipated. However, in the case of compact clusters, the high atomic connectivity can cancel or render negligible the expected Jahn–Teller distortion, leading to stability for electron counts not satisfying the closed-shell principle.

We have recently reported on the electron-sponge behavior of cluster anions $[Co_{11}Te_7(CO)_{10}]^{n-}$ ($[\mathbf{1}]^-$) and $[Co_{11}Te_5(CO)_{15}]^{n-}$ ($n = 1,2$) built up of the pentagonal-prismatic $Co@Co_{10}$ polyhedron and shells of μ_4- and μ_5-Te bridges and terminal or bridging CO groups (Figure 1).[4,5] These anions form in the reaction of $[Cp^*_2NbTe_2H]$ ($Cp^* = C_5Me_5$) with $[Co_2(CO)_8]$. The appropriate cation is the very stable $[Cp^*_2Nb(CO)_2]^+$. A salt containing the hexacapped cubic $[Co_9Te_6(CO)_8]^{2-}$ anion formed also in this reaction, but could be established only crystallographically (Figure 1).[5a] Electron-sponge properties were expected for this compound but could not yet be verified because of the lack of pure material.

The search for related cluster salts containing the Cp′ ($Cp' = tBuC_5H_4$) ligand was obviously handicapped by insufficient stability of the still elusive $[Cp'_2Nb(CO)_2]^+$ cation.[7] A first hint for the formation of $[Co_9Te_6(CO)_8]^{n-}$ con-

[a] Departement de Chimie, Faculté des Sciences Exactes, Université Mentouri-Constantine,
25000 Constantine, Algeria
[b] Sciences Chimiques de Rennes (UMR 6226), Université de Rennes 1,
35042 Rennes Cedex, France
[c] Institut de Chimie Moléculaire de l'Université de Bourgogne ICMUB-UMR CNRS 5260, Faculté des Sciences Mirande, Université de Bourgogne,
21100 Dijon, France
[d] Institut für Anorganische Chemie, Universität Regensburg,
93040 Regensburg, Germany
E-mail: joachim.wachter@chemie.uni-regensburg.de
Supporting information for this article is available on the WWW under http://www.eurjic.org or from the author.

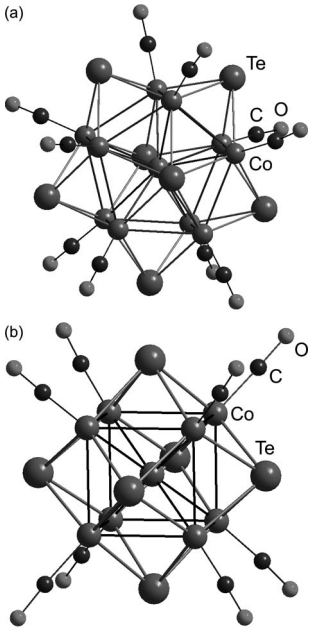

Figure 1. Structural motifs of $[\mathbf{1}]^{n-}$ (**a**) and $[\mathbf{3}]^{n-}$ (**b**) (n = 1,2) anions.[5,6]

taining salts was obtained in the reaction of $[Co_2(CO)_8]$ with CH_3Li-reduced $[Cp'_2NbTe_2H]$ (**2**),[8,9] which proceeds via highly reactive intermediates.[10]

In this work we describe the preparation and supramolecular structures of the salts $[PPN]_n[\mathbf{3}]$ {PPN = Ph_3PNPPh_3; **3** = $[Co_9Te_6(CO)_8]$; n = 1,2}, which complete the product variety in the reaction sequence **2**/CH_3Li/$[Co_2(CO)_8]$. We also report on the redox behavior of the $[\mathbf{3}]^-$ anion, its magnetic properties and the electron structures of differently charged $[\mathbf{3}]^{n-}$ (n = +1 to –5) clusters, and reactivity studies on salts containing $[\mathbf{3}]^-$ are described.

Results and Discussion

Synthesis and Characterization

The reaction of the solution of **2** in THF with two equivalents of CH_3Li at room temperature proceeds via formation of, among others, $[Cp'_2Nb(Te)CH_3]$, $[Cp'_2Nb(H)_2TeCH_3]$, and $[Cp'_2Nb(TeCH_3)_2]$.[10] Subsequent addition of $[Co_2(CO)_8]$ to the reduced solution gave neutral $[Co_9(\mu_4\text{-}TeR)_2(\mu_4\text{-}Te)_4(CO)_8]$ [R = $Cp'_2Nb(CO)$] and $[Cp'_2Nb(\mu\text{-}TeCH_3)_2Co(CO)_2]$[10] along with a slightly oily mixture. This mixture was supposed to contain ionic compounds of composition $[Li]_n[Co_9Te_6(CO)_8]$ (n = 1, 2). Salt metathesis of the latter with $[PPh_4]Cl$ gave products that were obstinately contaminated by $[PPh_4]Cl$.

Dissolving the brown $[Li]_n[\mathbf{3}]$ mixture in aqueous ethanol and stirring with excess [PPN]Cl (PPN = Ph_3PNPPh_3) gave a voluminous precipitate. The IR spectrum of the crude material reveals a strong ν(CO) absorption at 1890 cm^{-1}, typical of the dianionic cluster, and a comparably weak band at 1935 cm^{-1}, characteristic of the monoanionic cluster. This means, following a correlation of the ν(CO) absorptions with the charge (see below), that the crude precipitated salt consists mainly of $[PPN]_2[\mathbf{3}]$.

Recrystallization of $[PPN]_n[\mathbf{3}]$ (n = 1,2) from CH_2Cl_2 gave dark needles of [PPN][**3**] in about 28% yield (with respect to **2**). This yield was obtained by repeated precipitation of crystalline material from the mother liquors. The IR spectrum shows one strong ν(CO) absorption at 1935 cm^{-1}, elemental analysis is in agreement with a 1:1 salt. Only in one case a few crystals of $[PPN]_2[\mathbf{3}]$ were isolated in low quantity, which was not sufficient for complete characterization. These observations support the electrochemical finding that there is a slow conversion of $[\mathbf{3}]^{2-}$ to $[\mathbf{3}]^-$ in solution (see below).

The NI-ESI-MS of analytically pure [PPN][**3**] reveals a peak centered at m/z 1520.1 (I 100%) characteristic of $[\mathbf{3}]^-$. Another peak at m/z 760.7 corresponds to the dianion $[Co_9Te_6(CO)_8]^{2-}$. The intensity ratio between both peaks is dependent on the capillary temperature.[8]

The crystal structure of [PPN][**3**] contains in the triclinic cell one pair of $[PPN]^+$ and $[\mathbf{3}]^-$ ions in the molecular unit (Figure 2). The structure of the cluster anion is composed of a Co_8 cube with an interstitial Co atom, six capping μ_4-Te ligands and terminal CO ligands at each of the Co vertices. The bond parameters of $[\mathbf{3}]^-$ are typical of the 122-MVE cluster anion (Table 1).[8] As in $[Na(THF)_6][\mathbf{3}]$ a distorted CsCl lattice is observed. This kind of packing may be promoted by overall diameters of cations (ca. 10.6 Å) and anions (12.6–12.8 Å) of approximately the same order. The linear P–N–P arrangement along with the staggered conformation of the phenyl groups in the cation results in optimum space-filling. A further stabilization effect may be ascribed to C–H···O interactions between phenyl hydrogens and CO ligands in the range of 2.5–2.8 Å (Figure 2). The importance of this kind of hydrogen-bonding for crystal packing has been discussed elsewhere.[11,12] In our case it may be intensified by electrostatic forces.

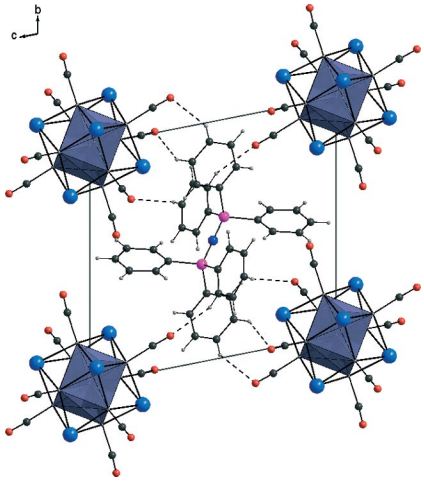

Figure 2. Projection of the unit cell of [PPN][**3**] on the *bc* plain, with O···H interactions between 2.50 and 2.80 Å as dotted lines; grey: Co, blue: Te, red: O, black: C, dark blue: N, violet: P.

Table 1. Comparison of important bond lengths [Å] of [PPN][**3**], $[PPN]_2$[**3**], **4** and **5**·3Cr(CO)$_5$.

	4	[PPN][**3**]	$[PPN]_2$[**3**]	**5**·3Cr(CO)$_5$[7]
MVE[a]	121	122	123	124
μ_4-Te–Co	2.520(3)–2.543(3)	2.519(2)–2.538(2)	2.525(1)–2.539(1)	2.474(3)–2.505(3)
Te–Co_{centr}	2.974(4), 2.9874(4)	2.980(2)–2.981(2)	2.979(1), 2.999(1)	2.912(4)–2.956(5)
Co–Co	2.769(4)–2.797(4)	2.773(2)–2.793(3)	2.759(1)–2.793(1)	2.741(8)–2.778(9)
Co–Co_{centr}	2.395(4)–2.428(8)	2.401(2)–2.414(2)	2.399(1)–2.405(1)	2.381(6)–2.412(5)
P–N		1.568(4)	1.586(3)	
Co–P	2.199(8), 2.228(9)			

[a] Metal valence electrons.

Crystals of $[PPN]_2$[**3**] were accidentally obtained in the first fraction. The IR spectrum exhibits a strong ν(CO) absorption at 1885 cm^{-1}, thus serving as a reference frequency for [**3**]$^{2-}$. X-ray diffraction analysis shows that the monoclinic cell is composed of two molecular units and each molecular unit contains two $[PPN]^+$ cations and one [**3**]$^{2-}$ dianion (Figure 3). The Co_9Te_6 cube contains an inversion center. The bond parameters of the 123-MVE cluster (Table 1) are similar to those in [PPN][**3**]. The only striking difference between both structures is the bent $[PPN]^+$ cation with a P–N–P angle of 141°, and the phenyl rings are arranged in an eclipsed conformation. The resulting packing may be described by undulated 2-D layers of cations being well separated by the large anions (Figure 3). The different packing in $[PPN]_2$[**3**] and [PPN][**3**] demonstrates for the first time that the crystal lattice may be affected by the charge of the cluster anion. This finding is in striking contrast to the supramolecular chemistry of PPN salts in which the individual cationic structure motif is unaffected by the charge of the anion.[13]

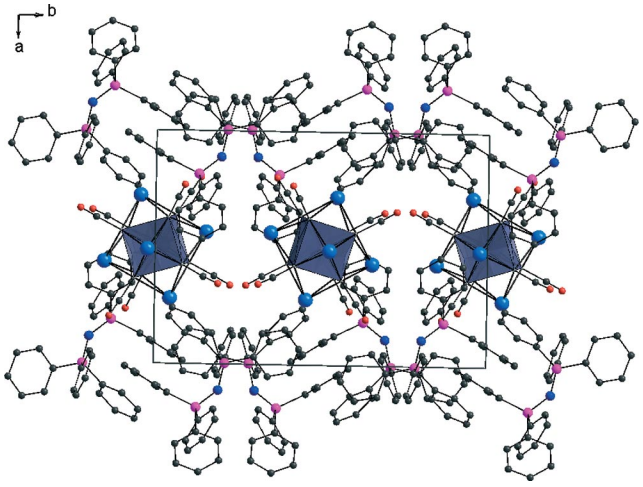

Figure 3. Crystal packing repeat of $[PPN]_2$[**3**], view down the *c* axis. The grey cubes symbolize the Co@Co_8 polyhedron, the meaning of the other colors is the same as in Figure 2.

Cluster Reactivity

Following the CO-substitution/cluster-oxidation pathway of the reaction of phosphanes with [**1**]$^{n-}$ anions,[5b] the formation of neutral PR_3-substituted clusters was attempted by reacting $[Cp^*_2Nb(CO)_2]$[**3**] with bis(diphenylphosphanyl)ethane (dppe). Whereas at room temperature there was no reaction, in boiling THF $[\{Co(CO)_2(dppe)\}_2(\mu\text{-Te})]$ formed among other, not identified compounds. From X-ray crystallography the molecular structure consists of two trigonal-pyramidal $Co(CO)_2$(dppe) moieties being linked by a Te bridge.[14] As it was impossible to separate the different products either by chromatography or by crystallization reasonable spectroscopic data are not available.

Surprisingly, a cluster compound of composition $[Co_9Te_6(CO)_4(PPh_3)_4]$ (**4**), (Figure 4) was obtained from the reaction of $[Cp^*_2Nb(CO)_2]$[**1**] with PPh_3AuCl in boiling THF. The compound is extremely air-sensitive in solution and under FD mass spectrometric conditions. The IR spectrum reveals one strong CO stretching frequency at 1922 cm^{-1}. Single crystals were obtained by recrystallization, but always contaminated by varying amounts of grey tellurium powder. For this reason no sufficient analysis is available. The important bonding parameters of **4** are closely related to those of [**3**]$^-$ and [**3**]$^{2-}$ anions (Table 1). The corresponding relation between cluster charge and distances will be discussed below. As by-product $[Cp^*_2Nb(CO)_2][PPh_3CoCl_3]$ was obtained as green needles by direct recrystallization of the reaction mixture.[14]

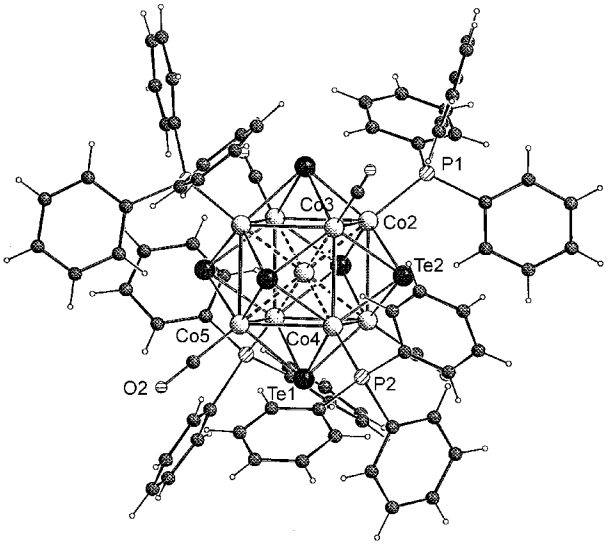

Figure 4. Structure of $[Co_9Te_6(CO)_4(PPh_3)_4]$ (**4**). A threefold axis passes through P(1), Co(2), Co(1), Co(5) and O(2); the interstitial Co atom is Co(1).

The formation of **4** is unprecedented in that a pseudo-protonation[15] of one of the nucleophilic μ_5-Te bridges of the $Co_{11}Te_7$ skeleton was expected. However, attempts to prepare neutral analogues of **4** from [**3**]$^-$ salts and

PPh_3AuCl gave a mixture containing blue $[(PPh_3)_2Au][CoCl_3PPh_3]$,[14] green $[Cp^*_2Nb(CO)_2][PPh_3CoCl_3]$ (see above) and black microcrystalline material of still unknown nature. The formation of the Te-free anions may be explained by the easy and irreversible oxidation of the cluster core as found in electrochemical experiments (see below). It may be noted that pseudo-protonated clusters with the $Co@Co_8Te_6$ core exist (Scheme 1): $[Co_9Te_4\{\mu_5\text{-}Cp'_2Nb(CO)Te\}_2(CO)_8]$[8] is one of the products of the title reaction described previously,[8] whereas $[Co_9Te_3\{\mu_5\text{-}Cp'_2Nb(CO)Te\}_3(CO)_8]$ (**5**) forms in the reaction of **2** with $[Co_2(CO)_8]$ in boiling toluene.[7]

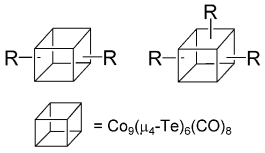

Scheme 1. Schematic representation of pseudo-alkylated $Co_9Te_6(CO)_8$ cluster derivatives with R = $Cp'_2Nb(CO)$.

Electrochemical Investigations

In a previous work we have shown that the pentagonal-prismatic $[Co_{11}Te_7(CO)_{10}]$-skeleton behaves like an electron-sponge.[5] Such properties have also been predicted for $[\mathbf{3}]^-$ but could not be verified due to lack of material.[8] The isolation of analytically pure $[Cp^*_2Nb(CO)_2][\mathbf{3}]$ by chromatography on SiO_2 allowed us to investigate its electrochemical properties by using cyclic voltammetry, rotating disk electrolysis (RDE) voltammetry and electrolysis methods.

The cyclic voltammogram of $[Cp^*_2Nb(CO)_2][\mathbf{3}]$ on carbon electrode in THF contains six systems in the cathodic area: A_1/A'_1, A_2/A'_2, C_1/C'_1, C_2/C'_2, A_3/A'_3 and A_4/A'_4 with E_c = –0.38 V, –1.16 V, –1.43, –1.73, –1.97 and –2.48 V, respectively (Figure 5). When starting at –0.1 V, three irreversible oxidation peaks E'_1, E'_2 and E'_3 were found at +0.5, +0.75 and +1.24 V, respectively. The total height of waves E'_1, E'_2 and E'_3 is approximately ten times higher than that of wave A_1. After 9-e$^-$ oxidation (n_{exp} = 8.6 e$^-$) at the potential of wave E'_3 the color of the solution turned from maroon to almost colorless, which may be interpreted as oxidative degradation of the cluster anion. Indeed, cationic cobalt species have been found in diverse substitution reactions of $[Cp^*_2Nb(CO)_2][\mathbf{3}]$ (see above).

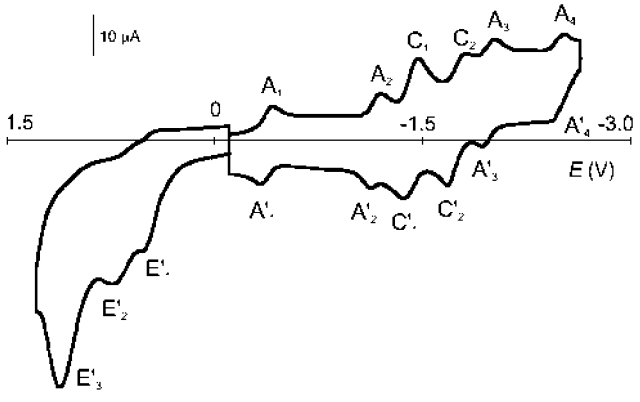

Figure 5. Cyclic voltammogram of $[Cp^*_2Nb(CO)_2][\mathbf{3}]$ on carbon electrode in THF (0.2 mol L^{-1} of $[NBu_4]PF_6$, scan rate 100 mV s^{-1}); starting potential –0.1 V.

The peaks A_1/A'_1, A_2/A'_2 and A_3/A'_3 may be assigned to the reversible reduction of $[\mathbf{3}]^-$ according to Equation (1), whereas peaks C_1/C'_1 and C_2/C'_2 are consistent with reversible reduction of the $[Cp^*_2Nb(CO)_2]^+$ cation. The system A_4/A'_4 is tentatively assigned to the reduction of $[\mathbf{3}]^{4-}$ which means that $[\mathbf{3}]^{5-}$ is sufficiently stable on the time scale of cyclic voltammetry. The corresponding RDE voltammograms are shown in Figure 7.

$$[\mathbf{3}]^- \underset{A_1/A'_1}{\overset{-0.38\ V}{\rightleftharpoons}} [\mathbf{3}]^{2-} \underset{A_2/A'_2}{\overset{-1.16\ V}{\rightleftharpoons}} [\mathbf{3}]^{3-} \underset{A_3/A'_3}{\overset{-1.97\ V}{\rightleftharpoons}} [\mathbf{3}]^{4-} \underset{A_4/A'_4}{\overset{-2.48\ V}{\rightleftharpoons}} [\mathbf{3}]^{5-} \quad (1)$$

This assignment is supported by the cyclic voltammogram of $[Na(THF)_6][\mathbf{3}]$, which exhibits only the systems A_1/A'_1, A_2/A'_2 and A_3/A'_3 (Figure 6). The peaks C_1 and C_2 are not observed, A_4 does not appear, instead Na^+ is reduced before. Other cations like $[PPh_4]^+$ (–1.68, –2.07 V[16]) or $[PPN]^+$ (–2.07 V in THF/DMF) exhibit reduction waves in the same range.

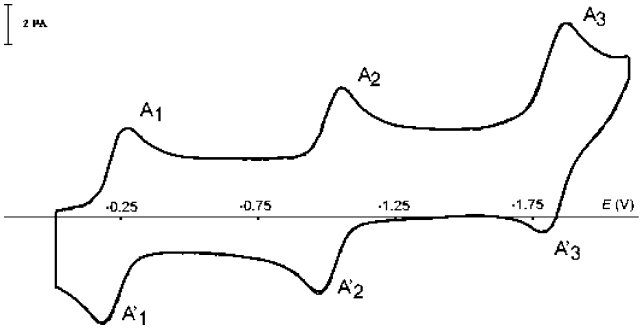

Figure 6. Cyclic voltammogram of $[Na(THF)_6][\mathbf{3}]$ on carbon electrode in THF.

Electrolysis of $[Cp^*_2Nb(CO)_2][\mathbf{3}]$ at –0.7 V (plateau of wave A_1) consumes 1 F (n_{exp} = 0.97 F). The RDE voltammogram of the resulting solution exhibits the oxidation wave A'_1 and the reduction waves A_2, C_1, C_2 and A_3 (Figure 7, b). This result is in agreement with the quantitative formation of the dianion according to the reaction $[\mathbf{3}]^- + e^- \rightarrow [\mathbf{3}]^{2-}$. The dianion is very stable since no evolution occurs even after several hours. Further electrolysis at –1.3 V (plateau of wave A_2) gives after consumption of 0.5 F an RDE voltammogram which exhibits oxidation wave A'_1 and reduction waves A_2, C_1, C_2 and A_3. Interestingly, the height of wave C_1 has decreased (Figure 7, c). This result suggests that the electrogenerated trianion [Equation (2a)] interacts with the $[Cp^*_2Nb(CO)_2]^+$ cation [Equation (2b)].

$$[\mathbf{3}]^{2-} + e^- \rightleftharpoons [\mathbf{3}]^{3-} \quad (2a)$$

$$[\mathbf{3}]^{3-} + [Cp^*_2Nb(CO)_2]^+ \rightleftharpoons [\mathbf{3}]^{2-} + \text{“}Cp^*_2Nb(CO)_2\text{”} \quad (2b)$$

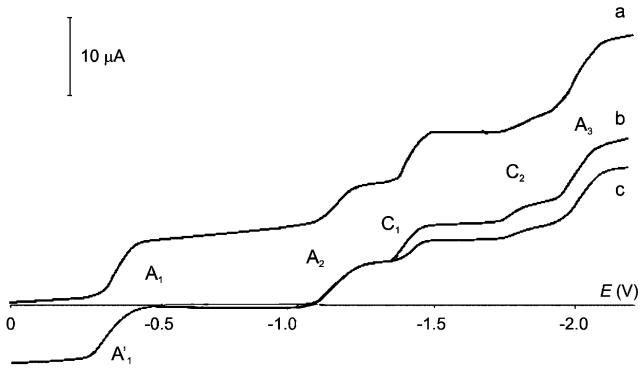

Figure 7. RDE voltammogram of $[Cp^*_2Nb(CO)_2]$[**3**] on carbon electrode in THF (0.2 mol L^{-1} of $[NBu_4]PF_6$; scan rate 20 mV s^{-1}): (a) initial voltammogram; (b) after electrolysis at –0.7 V and consumption of one electron; (c) after electrolysis at –1.3 V and consumption of 0.5 F.

Reaction (2b) is thermodynamically unfavorable but can be explained by an outer-sphere electron-transfer reaction since the potential difference of 0.27 V between C_1 and A_2 is small. The resulting neutral "$Cp^*_2Nb(CO)_2$" is supposed to be unstable because of its 19-e^- configuration. A similar transfer reaction has been postulated for the interaction of $[\mathbf{1}]^{3-}$ with $[Cp^*_2Nb(CO)_2]^+$.[5a]

Reduction of $[\mathbf{3}]^-$ at –1.7 V consumes 3 F (n_{exp} = 2.96 F). The resulting solution exhibits an RDE voltammogram with two oxidation waves A'_1 and A'_2 and one reduction wave A_3,[17] which are characteristic of the quantitative formation of the trianion [Equation (3)]. The trianion $[\mathbf{3}]^{3-}$ is moderately stable even in the presence of additional water.

$$[Cp^*_2Nb(CO)_2][\mathbf{3}] + 3\ e^- \rightleftharpoons [\mathbf{3}]^{3-} + "Cp^*_2Nb(CO)_2" \quad (3)$$

When the reduction of monoanion is performed at –2.2 V (plateau of wave A_3) the current decreases from 0.7 mA to 0.2 mA. Then it is stable even after consumption of an important quantity of electricity (n_{exp} = 11.9 F). By RDE voltammetry, only waves A'_1, A_2 and A_3 are present indicating that the dianion is formed.[17] As wave A'_2 appears with very low intensity, the trianion is also observed in trace amounts. The quantity of electricity consumed may be seen as the beginning of a catalytic process where the tetraanion reduces a substrate present in solution ($[NBu_4]^+$ or residual water). This first hypothesis cannot be verified using $NaBPh_4$ instead of $[NBu_4]PF_6$ since Na^+ is reduced, as mentioned above, at a less negative potential than –2.2 V. In the presence of additional water, no modification of waves A_1 and A_2 are observed, but the height of the wave A_3 increases in agreement with a fast reactivity of the tetraanion towards water.

In summary, the anionic species $[\mathbf{3}]^n$ (n = –1 to –4) are stable on the time scale of CV. In contrast only the dianionic species is very stable on the time scale of electrolysis. The trianion generated from electrolysis is moderately stable even in the presence of water, whereas the tetraanion is very unstable.

Electronic Structures of $[\mathbf{3}]^n$

Differently charged and substituted carbonyl cobalt telluride clusters belonging to the type of cubic M_8 polyhedral geometry are described. Electrochemical studies reveal the presence of the anionic species $[\mathbf{3}]^n$ (n = –1 to –5) in solution. The corresponding electron counts are 122 to 126 MVE. Although there is no electrochemical proof of a 121-MVE cluster, an uncharged species $[\mathbf{3}]^0$ may be obtained by degradation of the $Co_{11}Te_7$ of $[\mathbf{1}]^-$ and concomitant substitution of four CO by PPh_3 ligands. By this way, crystallographic data are now available for clusters with 121, 122 and 123 MVE. This range may be extended to 124 MVE with $[Co_9Te_3\{\mu_5\text{-}Cp'_2Nb(CO)Te\}_3(CO)_8\cdot 3Cr(CO)_5]$ {[**5**·$3Cr(CO)_5$]}, which is a pseudo-protonated derivative of the $[\mathbf{3}]^{3-}$ anion. The cluster bears three additional $Cr(CO)_5$ fragments for the purpose of better crystallization (Figure 8).

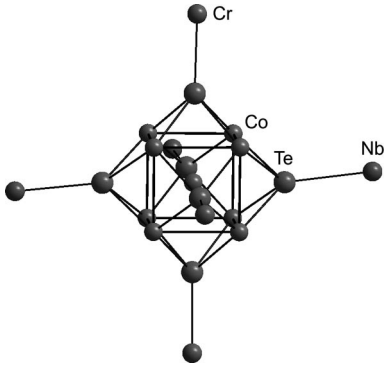

Figure 8. Co_9Te_6-core of [**5**·$3Cr(CO)_5$] with attached "Cr" and "Nb", that symbolize $Cr(CO)_5$ and $Cp'_2Nb(CO)$ fragments.[7]

Previous theoretical investigations of the electronic structure of transition-metal centered cubic clusters of the type $M_9(\mu_4\text{-}E)_6L_8$ (M = Ni, Pd; E = GeEt, As, Te) have shown that the best favored closed-shell electron count for such species is 124 MVE.[1b–1d] This situation (Figure 9) originates from the best closed-shell electron count of the non-centered $M_8(\mu_4\text{-}E)_6L_8$ species which is 120 MVE. With this electron count, a significant HOMO–LUMO gap is generally found for $M_8(\mu_4\text{-}E)_6L_8$ clusters.[1a] When an additional metal atom is placed in the middle of the cube, only three (of t_{2g} symmetry) among its five low-lying d-type orbitals can significantly interact with low-lying counterparts on the $M_8(\mu_4\text{-}E)_6L_8$ cage. Indeed, contrarily to the e_g manifold, these three AOs provide a good overlap match with the M_8 cube. As a result, the e_g d-type AOs of the central metal are weakly perturbed and remain at low energy. Thus, the closed-shell principle requires their occupation, leading to the MVE count of 120 (empty cage) + 4 (central M) = 124, the corresponding electron configuration being in the following noted $[120](e_g)^4$. A typical example of this closed-shell count is $Ni_9(\mu_4\text{-}GeEt)_6(CO)_8$.[18] However, it has also been shown that in the particular case where E is a bare main-group atom, the 124-MVE closed-shell configuration is not always ensured, due to the lone

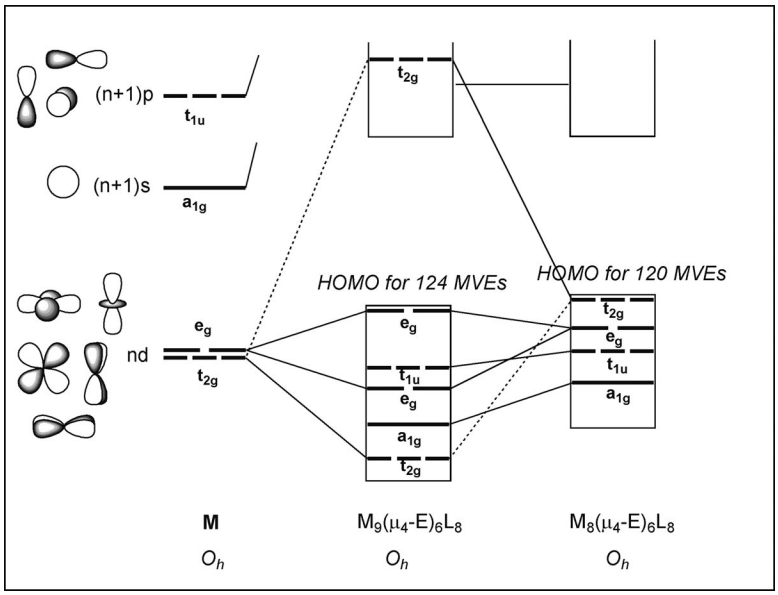

Figure 9. Schematic interaction MO diagram between the frontier orbitals of an $M_8(\mu_4\text{-E})_6L_8$ cage and its μ_8-M host. In the more general case, the best favored MVE counts (large HOMO–LUMO gaps) are 120 and 124 for the empty $M_8(\mu_4\text{-E})_6L_8$ and the centered $M_9(\mu_4\text{-E})_6L_8$ clusters, respectively.

pair effect of the bare μ_4-E atom. Indeed, these lone pairs, which span into $a_{1g}+t_{1u}+e_g$ combinations in the cluster O_h symmetry, tend to destabilize the occupied cluster levels of the same symmetries, especially in the case of heavy main-group E atoms which have diffuse lone pairs, able to provide long distance overlap. As a result, the HOMO–LUMO gap is reduced, with a high-lying e_g HOMO which in some cases can cross the LUMO and transfer its electrons into it.[1b] Alternatively, significant destabilization of this e_g orbital may favor its depopulation, i.e., favor the 120-MVE closed-shell configuration $[120](e_g)^0$, secured by the existence of a substantial HOMO–LUMO gap.

These previous results were obtained from calculations on Group 10 clusters.[1b] We have first in the present work tested their validity for the less electronegative cobalt case by carrying out DFT calculations on the $[\mathbf{3}]^n$ (n = +1 to –5) series and then on closely related species. The MO diagram of the 124-MVE anion $[\mathbf{3}]^{3-}$ is shown in Figure 10 and some important computed data are given in Table 2. The ground-state level occupation corresponds to the above predicted electronic configuration $[120](e_g)^4$ and is consistent with the qualitative diagram of Figure 9. However, the computed HOMO(e_g)–LUMO(t_{1g}) gap is not very large (0.32 eV) and the triplet state is computed to be only 0.39 eV less stable than the singlet state. Clearly, the rather high energy of the e_g HOMO results from the E = Te lone-pair effect described above. This is also exemplified by the plots of the e_g HOMOs (Figure 10) which show Co(central)–Te antibonding character. Similar results, i.e., a singlet ground state associated with a moderate HOMO–LUMO gap were found for the 124-MVE cluster $[Co_9(Te)_6(CO)_4(PH_3)_4]^{3-}$ ($[\mathbf{4}']^{3-}$) taken as a simplified model for a hypothetical reduced form of **4** (see Table 2).

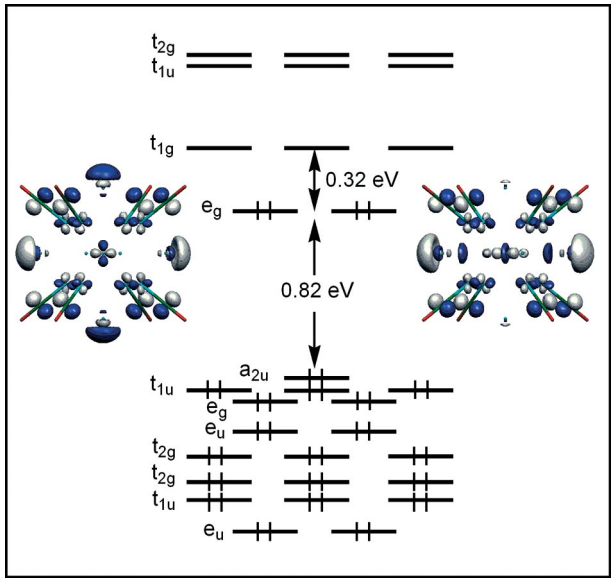

Figure 10. The MO diagram of $[\mathbf{3}]^{3-}$ (124 MVE) with plots of the e_g HOMOs.

The Te lone-pair effect in $[\mathbf{3}]^{3-}$ can be switched off by "complexing" the lone pairs, for example by H^+. The corresponding 124-MVE model $[Co_9(TeH)_6(CO)_8]^{3+}$ exhibits a substantial HOMO(e_g)–LUMO(t_{1g}) gap of 0.88 eV in its singlet ground-state, whereas its triplet state is computed to be 0.91 eV less stable. Complexing the Te lone pairs by $Cr(CO)_5$ groups, i.e., calculating $[Co_9\{TeCr(CO)_5\}_6(CO)_8]^{3-}$ leads to similar results, with a significant HOMO (e_g)–LUMO (t_{1g}) gap of 0.95 eV (Table 2). This computed model

Table 2. Selected data for the computed ground-states of the series $[Co_9Te_6(CO)_8]^n$ ([**3**]^n; n = +1 to –5) and related clusters; bond lengths are given in Å.

Compound (symmetry)	MVE	Electron configuration	Spin state	HOMO–LUMO gap	Co–Co (cube edge)	Co–Te	Co–C	C–O	Lowest vibrational frequency
$[Co_9Te_6(CO)_8]^+$, [**3**]$^+$ (O_h)	120	$[120](e_g)^0(t_{1g})^0$	s	0.67 eV	2.898	2.529	1.810	1.154	33 cm^{-1} (t_{1u})
$Co_9Te_6(CO)_8$, [**3**]^0 (O_h)	121	$[120](e_g)^1(t_{1g})^0$	d		2.886	2.535	1.791	1.161	46 cm^{-1} (t_{1u})
$[Co_9Te_6(CO)_8]^-$, [**3**]$^-$ (O_h)	122	$[120](e_g)^2(t_{1g})^0$	t		2.853	2.559	1.764	1.167	41 cm^{-1} (t_{2u})
$[Co_9Te_6(CO)_8]^{2-}$, [**3**]$^{2-}$ (O_h)	123	$[120](e_g)^3(t_{1g})^0$	d		2.843	2.569	1.759	1.176	55 cm^{-1} (t_{1u})
$[Co_9Te_6(CO)_8]^{3-}$, [**3**]$^{3-}$ (O_h)	124	$[120](e_g)^4(t_{1g})^0$	s	0.32 eV	2.851	2.574	1.756	1.184	54 cm^{-1} (t_{2u})
$[Co_9Te_6(CO)_8]^{4-}$, [**3**]$^{4-}$ (O_h)	125	$[120](e_g)^4(t_{1g})^1$	d		2.878	2.589	1.750	1.194	57 cm^{-1} (t_{1u})
$[Co_9Te_6(CO)_8]^{5-}$, [**3**]$^{5-}$ (O_h)	126	$[120](e_g)^4(t_{1g})^2(t_{2g})^0$	t		2.918	2.610	1.743	1.203	54 cm^{-1} (t_{2u})
$[Co_9Te_6(CO)_4(PH_3)_4]^0$, [**4′**] ($C_{3v}$)	121	$[120](e_1)^1(e_1)^0$	d		2.874[a]	2.543[a]	1.776[a] Co–P: 2.188[a]	1.165[a]	54 cm^{-1} (a_2)
$[Co_9Te_6(CO)_4(PH_3)_4]^{3-}$, [**4′**]$^{3-}$ (C_{3v})	124	$[120](e_1)^4(e_1)^0$	s	0.41 eV	2.833[a]	2.576[a]	1.756[a] Co–P: 2.135[a]	1.187[a]	56 cm^{-1} (a_2)
$[Co_9(TeH)_6(CO)_8]^{3+}$ (O_h)	124	$[120](e_g)^4$ $(t_{1g})^0$	s	0.88 eV	2.860	2.532	1.842	1.146	44 cm^{-1} (t_{2u})
$[Co_9\{TeCr(CO)_5\}_6(CO)_8]^{3-}$ (O_h)	124	$[120](e_g)^4(t_{1g})^0$	s	0.95 eV	2.818	2.561	1.783	1.166 Te–Cr: 2.865	not computed

[a] Average value.

is closely related to the structure of [**5**·3Cr(CO)$_5$], in which Te lone-pairs are alternatively complexed by Cp′$_2$Nb(CO) or Cr(CO)$_5$ moieties (Figure 8).[7]

We investigate now the electronic structure of the 120- to 126-MVE series [**3**]^n (n = +1 to –5). Selected computed data are provided in Table 2. The MO level ordering of the 120-MVE [**3**]$^+$ cation is similar to that of the 124-MVE [**3**]$^{3-}$ species and therefore has an empty e_g LUMO, i.e., the $[120](e_g)^0$ configuration. Its singlet ground-state is secured by a substantial HOMO–LUMO gap (0.67 eV). Thus, this hypothetical species should be diamagnetic. The 121- to 124-MVE species correspond to the occupation of the e_g level, i.e., to the configurations $[120]e_g^x$ (x = 1 to 4). Surprisingly, the O_h structure does not exhibit any Jahn–Teller instability in the cases of x = 1 and 3, as shown by the absence of any imaginary computed vibrational frequencies. Clearly, the high connectivity of the cluster prevents any (even weak) Jahn–Teller distortion, at least at the considered level of calculations. Small distortions away from the octahedral framework have not to be completely excluded however. This is suggested by our partial exploration of their potential energy surfaces which were found quite flat around their minimum and by the particularly small values of their lowest vibrational frequencies (Table 2). The 121-MVE cluster $[Co_9(Te)_6(CO)_4(PH_3)_4]$ ([**4′**]^0) taken as a simplified model for **4** was also computed (Table 2). It exhibits rather similar electronic and structural features as its isoelectronic relative [**3**]^0. The fact that **4** is more stable than the elusive [**3**]^0 species can be rationalized by the fact that the spin density is more concentrated on the interstitial Co atom in the case of **4** (1.02 and 1.15 for [**3**]^0 and [**4′**]^0, respectively) and by the steric protection offered by the phosphane ligands in the case of **4**.

Filling the e_g level results in a regular decrease of the Co–Co cube edge, due to the fact that this level is weakly bonding along this edge. Conversely, the distance between the encapsulated metal and the Te atoms increases due to the antibonding character of the corresponding contacts (Table 2). The 125- and 126-MVE species are computed to adopt the configuration $[120]e_g^4t_{1g}^x$ (x = 1 and 2) in their ground states. As for their 121- and 123-MVE relatives, they were found to be Jahn–Teller resistant. The 126-MVE cluster [**3**]$^{5-}$ is computed to have a triplet ground state. The singlet state is found to be only 0.15 eV above and also maintains the octahedral symmetry. Clearly, this [**3**]^n electron-sponge family does not want to change its connectivity upon changing its electron count. Going from 124 to 126 MVE results in the lengthening of both Co–Co and Co···Te contacts, in agreement with the weak antibonding character of the t_{1g} level on the corresponding contacts.

Magnetic Behavior of [PPN][3]

In order to get a better insight into the electronic structure of the [**3**]^n series, we have investigated the magnetic properties between 2 K and 300 K of [PPN][**3**]. At room temperature the compound is paramagnetic with an effective magnetic moment μ_{eff} = 4.65 μ_B. In considering the free electron Zeeman factor (g = 2.00), μ_{eff} is close to the value we can expect for isolated spin quintuplet (μ_{eff} = 4.90 μ_B) while calculations indicate a triplet ground state at 0 K. The quintuplet state was then calculated and found to be 0.96 eV above the ground state. On cooling, μ_{eff} decreases slowly down to 100 K, with a value still higher than that of the spin only value for a triplet state (2.83 μ_B), then it decreases more and more rapidly. The temperature dependence of the molar magnetic susceptibility, χ_M, is plotted in Figure 11.

On cooling, the susceptibility increases continuously but not monotonically. It is highly improbable that the shoulder which shows up at around 5 K is of intramolecular origin. Indeed, this would suggest that there is an intramolecular equilibrium between singlet and triplet states, the singlet sitting few Kelvin lower in energy than the triplet while calculations found that the singlet is 0.37 eV (≈ 4300 K) above

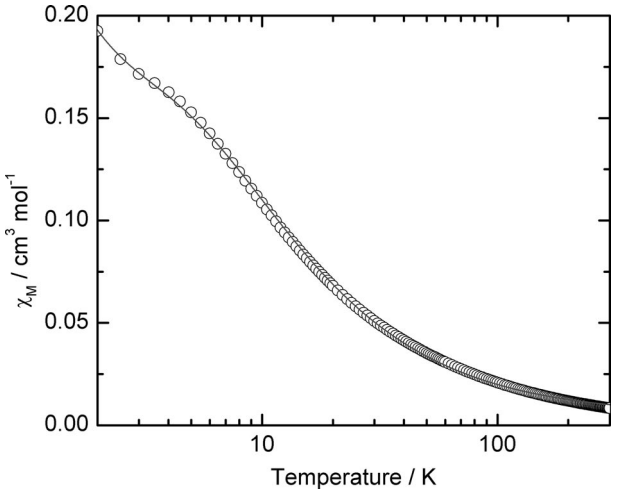

Figure 11. Temperature dependence of the molar magnetic susceptibility of a powdered sample of [PPN][**3**]; (o) experimental points (–) best fitted curve.

the triplet. Therefore, we conclude that the low temperature behavior is the result of antiferromagnetic intermolecular interactions. Looking at the crystal packing, short intermolecular contacts take place between Te2 atoms of neighboring clusters along the *a* axis. Indeed, the distance Te2–Te2 is equal to 4.051(23) Å while the van der Waals radius of tellurium is equal to 2.06 Å. Additionally the DFT calculations show that some spin density (≈ 0.11 electron) is located on the tellurium atoms. Then, direct spin-exchange can occur between clusters along the *a* axis. From a magnetic point of view the system may be described by chains of $S = 1$ spins antiferromagnetically coupled. The exchange Hamiltonian of a chain constituted by N spins within a magnetic field is written as

$$H = -\sum_{i=1}^{N-1} J\boldsymbol{S}_i \cdot \boldsymbol{S}_{i+1} + \sum_{i=1}^{N} g\beta \boldsymbol{H} \cdot \boldsymbol{S}_i$$

with J the exchange interaction parameter, $\boldsymbol{S}_i$ the spin operator at site i, g the Zeeman factor, β and $\boldsymbol{H}$ the Bohr magneton and the magnetic field respectively. For spins larger than ½, there is no analytical expression for $N \rightarrow \infty$ to describe the thermal dependence of the molar magnetic susceptibility. However, an expression (valid for $J < 0$) fitting the numerical results of ring chain calculations has been proposed for $S = 1$ (see equation).[19]

$$\chi_M = (1-x)\frac{Ng^2\beta^2}{kT}\frac{2.0+0.0194x+0.777x^2}{3.0+4.346x+3.232x^2+5.834x^3} + x\frac{Ng^2\beta^2}{3kT}S(S+1) + T.I.P.$$

with $x = \dfrac{|J|}{kT}$

In the equation we have included a temperature-independent contribution (*T.I.P.*). Also, it is necessary to include contributions x from paramagnetic entities, which are supposed to follow the Curie law, in order to take into account the increase of χ_M at very low temperature. The best agreement between theory and experiment is obtained with $|J| = 2.286 \pm 0.030$ cm^{-1}, $g = 2.500 \pm 0.007$, *T.I.P.* $= 4.93 \pm 0.01 \times 10^{-3}$ cm^3 mol^{-1} and $x = 12.0 \pm 0.3\%$ with $R^2 = 0.9992$. The fitted and experimental curves are in excellent agreement (Figure 11). The *T.I.P.* is very large with respect to values commonly observed for transition metal ions (about 10^{-5} cm^3 mol^{-1}).[20] However, such large values have been already reported in metal clusters.[21] The existence of low-lying excited states which can couple to the ground state through Zeeman perturbation can induce such large van Vleck contribution.[20] Also, the admixture between the ground state and excited states can give rise to g values significantly larger than 2.00 through spin-orbit coupling.[19] It should be noted that the meaning of x is more subtle than that of a simple sample pollution by paramagnetic impurities. Indeed, in the crystals incorporated dichloromethane is easily lost from the solid (especially under vacuum) inducing symmetry breaking in the chain structure and creating chain fragments of various lengths. The ends of the chain fragments, which can be considered as isolated paramagnetic centres at low temperature, are expected to contribute significantly to the overall magnetism.

Conclusions

In this work we have shown that reduction of [Cp′$_2$Nb(Te$_2$)H] with CH_3Li and the subsequent reaction [Co$_2$(CO)$_8$] in THF gave aside from [Cp′$_2$Nb(TeCH$_3$)$_2$Co(CO)$_2$] the salts Li$_n$[**3**] (n = 1, 2) which were transferred by metathesis reactions with [PPN]Cl into stable compounds crystallizing in supramolecular networks. The crystallographic study of the packing in both [PPN]$_2$[**3**] and [PPN][**3**] demonstrates that the crystal lattice is affected by the charge of the cluster anion. This finding is in striking contrast to the supramolecular chemistry of PPN salts in which the individual cation structure motif is unaffected by the charge of the anion.[13]

Electrochemical studies prove the existence of redox couples [**3**]$^-$/[**3**]$^{2-}$/[**3**]$^{3-}$/[**3**]$^{4-}$/[**3**]$^{5-}$ regardless of the nature of the cation. Whereas oxidation of [**3**]$^-$ proceeds under decomposition, a neutral derivative of [**3**]^0, **4**, was prepared by the unusual cluster degradation of the pentagonal-prismatic cluster [**1**]$^-$. Concomitantly, four CO groups were substituted by four PPh_3 ligands. The metal valence electron (MVE) counts for the members of the whole series range from 120 for [**3**]$^+$ to 126 MVE for [**3**]$^{5-}$. DFT calculations indicate that the octahedral architecture of the hexacapped centered cubic structure is conserved over all this range of electron counts. Most of these species have open-shell configuration. Because of the high molecular connectivity and of the weak bonding/antibonding nature of the frontier MOs, they do not afford any Jahn–Teller distortion. Such a situation is reminiscent of solid-state chemistry. Furthermore, this electron-sponge behavior is unique within the family of metal-centered hexacapped M$_9$(μ_4-E)$_6$L$_8$ clusters.[2] Magnetization measurements on [PPN][**3**] unambiguously reveal a triplet ground state for the 122-MVE

count with antiferromagnetic exchange type interaction in one dimension between clusters within the crystal structure.

Experimental Section

General: All procedures were carried out under N_2 using dry solvents and glove box and Schlenk techniques. Elemental analyses (C,H) were performed by the Mikroanalytisches Laboratorium, Universität Regensburg. IR spectra were obtained with a Bio Rad FTS 155 spectrometer. ESI mass spectra were measured on a ThermoQuestFinnigan TSQ 7000 spectrometer. Electrochemical experiments were carried out as described in ref.[5a,5b]

Computational Details: Density functional theory calculations were carried out using the Amsterdam Density Functional (ADF 2006) package developed by Baerends and co-workers,[22] assuming the Vosko–Wilk–Nusair parametrization[23] for the local density approximation of electron correlation and the nonlocal density approximation of Becke[24] and Perdew[25] (BP86) for the exchange and correlation energies, respectively. The standard TZP basis set of the ADF program[22] was used for the atoms constituting all the computed compounds. The frozen-core approximation was used to treat the core electrons. Full geometry optimization was carried out for all the computed species.[17] All the optimized geometries discussed in this paper (except that of $[Co_9\{TeCr(CO)_5\}_6(CO)_8]^{3-}$) were characterized as true minima on the potential energy hypersurface by calculations of normal mode vibrational frequencies (see Table 2).

Magnetic Measurements: The magnetizations have been recorded with a Quantum Design MPMS SQUID magnetometer operating in the temperature range 2–300 K with a DC magnetic field up to 5 T. The experimental data have been corrected from the diamagnetism of the sample holder and the intrinsic diamagnetism of the materials evaluated with Pascal's tables.

$[Cp^*_2Nb(CO)_2]$[3]: A mixture of $[Cp^*_2NbTe_2H]$ (329 mg, 0.53 mmol), $[Co_2(CO)_8]$ (342 mg, 1.00 mmol) and toluene was refluxed for 3 h. After cooling the dark precipitate was separated from the supernatant yellow solution and washed several times with toluene. Then, the dark brown residue was dissolved in CH_2Cl_2 (25 mL). Chromatography on SiO_2 (activity II/III; column 15×3 cm) gave after elution with CH_2Cl_2 red-brown $[Cp^*_2Nb(CO)_2]$[**1**].[5a] Continuous elution with a large volume of CH_2Cl_2 was applied until another red-brown band appeared containing analytically pure $[Cp^*_2Nb(CO)_2]$[**3**] (80 mg, 7.8%). Complex $[Cp^*_2Nb(CO)_2]$[**3**]: $C_{30}H_{30}Co_9NbO_{10}Te_6$ (1939.43): calcd. C 18.57, H 1.56; found C 18.53, H 1.60, NI-ESI-MS (from CH_3CN) 1521 $\{[Co_9{}^{128}Te_6(CO)_8]^-$ = 1520$\}$; PI-ESI-MS (from CH_3CN) 419.0 ($[C_{22}H_{30}NbO_2]^+$). IR (KBr): $\tilde{\nu}$ = 2014 m, 1936 cm^{-1} vs (ν_{CO}).

Preparation of $[PPN]_n$[3] (n = 1,2): Reaction of a THF solution (100 mL) of $[Cp'_2NbTe_2H]$ (300 mg, 0.50 mmol) with CH_3Li (0.7 mL, 1.1 mmol in diethyl ether) gave a red-violet solution,[10] to which $[Co_2(CO)_8]$ (342 mg, 1.0 mmol) was added under spontaneous gas evolution. Then, the dark mixture was refluxed for 18 h. After evaporation of the solvent the residue was dissolved in toluene/acetone (2:1; v/v) transferred to SiO_2 (column 20×3 cm) and eluted with the same mixture to remove $[Cp'_2Nb(TeCH_3)_2Co(CO)_2]$.[10] Elution with acetone gave a dark brown oily material (244 mg) composed of [Li][**3**] and some diacetone alcohol. Recrystallization of this oily material from THF gave $[Na(THF)_6][Co_9Te_6(CO)_8]$ in modest yield.[8] If this material was dissolved in 30 mL of ethanol and treated with a solution of [PPN]Cl (270 mg, 0.53 mmol) in H_2O (30 mL) a brown precitipitate formed, which was filtered and washed with H_2O (5×15 mL) and ether (2×5 mL) and then dried in vacuo. The remaining brown solid (362 mg) contains according to IR spectroscopy a mixture of $[PPN]_n$[**3**] (n = 1, 2). Recrystallization of this mixture from CH_2Cl_2 at –25 °C gave after 1 d a few crystals of $[PPN]_2$[**3**], while crystals of [PPN][**3**] were obtained from the mother liquor in subsequent fractions (total yield 100 mg, 28% with respect to **2**). [PPN][**3**]:

Table 3. X-ray crystallographic data for complexes [PPN][**3**], $[PPN]_2$[**3**] and **4**.

Formula	[PPN][**3**]·$2CH_2Cl_2$	$[PPN]_2$[**3**]·$2CH_2Cl_2$	$C_{76}H_{60}Co_9O_4P_4Te_6 \cdot 3C_7H_8$
M_w	2228.5	2767.0	2725.4
Crystal size /mm	$0.24 \times 0.16 \times 0.04$	$0.48 \times 0.16 \times 0.09$	$0.25 \times 0.18 \times 0.15$
Crystal system	triclinic	monoclinic	trigonal
Space group	$P\bar{1}$	$P2_1/c$	$R3c$
a /Å	9.300(1)	13.678(1)	20.748(2)
b /Å	12.701(2)	18.570(2)	
c /Å	13.194(2)	18.482(1)	39.162(2)
α /°	100.5(0)		
β /°	92.2(0)	107.9(0)	
γ /°	101.2(0)		120
V /Å^3	1498.8(4)	4467.7(6)	14599(2)
Z	1	2	6
$\rho_{calcd.}$ /g cm^{-3}	2.469	2.057	1.860
λ [Mo-K_α /Å]	0.71073	0.71073	0.71073
Instrument	STOE-IPDS	STOE-IPDS	STOE-IPDS
T /K	173	173	173
Scan range	$2.06 < \Theta < 25.67$	$1.91 < \Theta < 25.86$	$2.51 < \Theta < 25.91$
Reflections collected	10870	37945	44911
Reflections unique	5302	8297	6265
Reflections observed [$I > 2\sigma(I)$]	3108	6948	3706
Parameters refined	346	526	315
Absorption correction	none	numerical	analytical
Transmission	0.808/0.349	0.728/0.508	0.684/0.527
Max./min. residual density /e Å^{-3}	2.226/–1.597	1.415/–0.769	1.226/–0.708
$R1$	0.063	0.029	0.080
$wR2$	0.168	0.057	0.083

$C_{44}H_{30}Co_9NO_8P_2Te_6$ (2056.7): calcd. C 25.67, H 1.47; found C 25.68, H 1.92. NI-ESI-MS (from CH_3CN; tube lens 32 V) 1520.1 {I = 100%; $[Co_9{}^{128}Te_6(CO)_8]^-$ = 1520}, 760.7 {I = 91%; $[Co_9{}^{128}Te_6(CO)_8]^{2-}$}. IR (KBr): $\tilde{\nu}$ = 1935 cm^{-1} vs (ν_{CO}). Spectral data for $[PPN]_2$[**3**]: IR (KBr): $\tilde{\nu}$ = 1884 cm^{-1} vs (ν_{CO}).

Reaction of $[Cp^*_2Nb(CO)_2]$[1] with PPh_3AuCl: A THF (30 mL) solution of $[Cp^*_2Nb(CO)_2]$[**1**] (200 mg, 0.09 mmol) was slowly dropped to the solution PPh_3AuCl (80 mg, 0.16 mmol) in THF (20 mL). The mixture was refluxed for 18 h and the solvent removed in vacuo after cooling to room temperature. The brown mixture was dissolved in toluene (20 mL) to give a soluble fraction and an insoluble residue. Chromatography of the soluble part (SiO_2; column 15 × 3 cm) gave upon elution with toluene a brown band containing **4**. Black prisms were obtained from toluene at –24 °C. The residue was dissolved in acetone (5 mL) and then layered with pentane (5 mL). Recrystallization at –24 °C gave green needles of $[Cp^*_2Nb(CO)_2][PPh_3CoCl_3]$ along with attached small cubes of $[Co_6(CO)_3(PPh_3)_3Te_8]$, both identified crystallographically. $[Cp^*_2Nb(CO)_2][PPh_3CoCl_3]$: $C_{40}H_{45}Cl_3CoNbO_2P$ (847.0): NI-ESI-MS (from acetone) 163.8 ($[CoCl_3]^-$ = 163.8), PI-NI-ESI-MS (from acetone) 419.1 ($[C_{22}H_{30}NbO_2]^+$). IR (KBr): $\tilde{\nu}$ = 2014 s, 1950 cm^{-1} vs (ν_{CO}).

Crystal Structure Determination of [PPN][3], $[PPN]_2$[3] and 4: Crystal data and details of the measurements are summarized in Table 3. The structures were solved by direct methods and least-squares refinement. The program package SHELXTL PLUS - Release 4.2/800 was employed using all unique reflections. Non-hydrogen atoms were refined anisotropically, and hydrogen atoms were added in calculated positions.

CCDC-601485 (for $[PPN]_2$[**3**]), -601486 (for [PPN][**3**]) and -670174 (for **4**) contain the crystallographic data (excluding structure factors). These data can be obtained free of charge from The Cambridge Crystallographic Data Centre via www.ccdc.cam.ac.uk/data_request/cif.

Supporting Information (see also the footnote on the first page of this article): Cartesian coordinates for all the optimized structures and RDE voltammograms of $[Cp^*_2Nb(CO)_2]$[**3**] after three and twelve electron reduction.

Acknowledgments

We are grateful to S. Dalmolin for her electrochemical technical assistance. We gratefully acknowledge support from the Deutsche Forschungsgemeinschaft (DFG). The theoretical part of this work was supported by a grant of the French-Algerian Comité Mixte d'Evaluation et de Perspective (CMEP/02MDU552) and by a grant from the Algerian Government for an 18-month stay of F. Z. T. in Rennes. J. Y. S. thanks the Institut Universitaire de France (IUF) for its support. Calculations were carried out at the French national computing center IDRIS (Orsay).

[1] a) E. Furet, A. Le Beuze, J.-F. Halet, J.-Y. Saillard, *J. Am. Chem. Soc.* **1994**, *116*, 274; b) E. Furet, A. Le Beuze, J.-F. Halet, J.-Y. Saillard, *J. Am. Chem. Soc.* **1995**, *117*, 4936; c) J.-F. Halet, J.-Y. Saillard, *Struct. Bonding (Berlin)* **1997**, *87*, 81; d) R. Gautier, J.-F. Halet, J.-Y. Saillard, in *Metal Clusters in Chemistry*, (Eds.: P. Braunstein, L. A. Oro, P. R. Raithby), Wiley-VCH, Weinheim, **1999**, vol. 3, 1643; e) T. P. Fehlner, J.-F. Halet, J.-Y. Saillard, *Molecular Clusters. A Bridge to Solid State Chemistry*, Cambridge University Press, Cambridge, UK, **2007**, p. 198.
[2] a) D. Fenske, J. Ohmer, K. Merzweiler, *Angew. Chem. Int. Ed. Engl.* **1988**, *27*, 1512; b) D. Fenske, H. Fleischer, C. Persau, *Angew. Chem. Int. Ed. Engl.* **1989**, *28*, 1665; c) D. Fenske, C. Persau, *Z. Anorg. Allg. Chem.* **1991**, *593*, 61; d) J. P. Zebrowski, R. K. Hayaski, A. Bjarnason, L. F. Dahl, *J. Am. Chem. Soc.* **1992**, *114*, 3121; e) J. G. Brennan, T. Siegrist, S. M. Stuczinski, M. L. Steigerwald, *J. Am. Chem. Soc.* **1989**, *111*, 9240.
[3] G. Longoni, C. Femoni, M. C. Iapalucci, P. Zanello, in *Metal Clusters in Chemistry* (Eds.: P. Braunstein, L. A. Oro, P. R. Raithby), Wiley-VCH, Weinheim, **1999**, vol. 3, 1137.
[4] O. Cador, H. Cattey, J.-F. Halet, W. Meier, Y. Mugnier, J. Wachter, J.-Y. Saillard, B. Zouchoune, M. Zabel, *Inorg. Chem.* **2007**, *46*, 501.
[5] a) H. Brunner, D. Lucas, T. Monzon, Y. Mugnier, B. Nuber, B. Stubenhofer, A. C. Stückl, J. Wachter, R. Wanninger, M. Zabel, *Chem. Eur. J.* **2000**, *6*, 493; b) H. Brunner, H. Cattey, W. Meier, Y. Mugnier, A. C. Stückl, J. Wachter, R. Wanninger, M. Zabel, *Chem. Eur. J.* **2003**, *9*, 3796.
[6] R. Seidel, R. Kliss, S. Weissgräber, G. Henkel, *J. Chem. Soc. Chem. Commun.* **1994**, 2791.
[7] H. Brunner, A. C. Stückl, J. Wachter, R. Wanninger, M. Zabel, *Angew. Chem. Int. Ed.* **2001**, *40*, 2463.
[8] A. Ebner, J. Wachter, M. Zabel, *J. Cluster Sci.* **2004**, *15*, 163.
[9] H. Brunner, A. Ebner, J. Wachter, M. Zabel, *C. R. Chim.* **2005**, *8*, 1856.
[10] A. Ebner, W. Meier, Y. Mugnier, J. Wachter, *Inorg. Chim. Acta* **2007**, *360*, 3330.
[11] a) B. K. Roland, H. D. Selby, J. R. Cole, Z. Zheng, *Dalton Trans.* **2003**, 4307; b) T. Fujimura, H. Seino, M. Hidai, Y. Mizobe, *J. Organomet. Chem.* **2004**, *689*, 738.
[12] a) D. Braga, F. Grepioni, G. R. Desiraju, *J. Organomet. Chem.* **1997**, *548*, 33; b) G. R. Desiraju, *J. Chem. Soc. Dalton Trans.* **2000**, 3745.
[13] G. R. Lewis, I. Dance, *J. Chem. Soc. Dalton Trans.* **2000**, 299.
[14] M. Zabel, personal communication.
[15] L. C. Roof, D. M. Smith, G. W. Drake, W. T. Pennington, J. W. Kolis, *Inorg. Chem.* **1995**, *34*, 337.
[16] L. Horner, J. Haufe, *J. Electroanal. Chem.* **1969**, *20*, 245.
[17] See supporting information.
[18] J. P. Zebrowski, R. K. Hayashi, A. Bjarnason, L. F. Dahl, *J. Am. Chem. Soc.* **1992**, *114*, 3121.
[19] A. Meyer, A. Gleizes, J. J. Gired, M. Verdaguer, O. Kahn, *Inorg. Chem.* **1982**, *21*, 1729.
[20] O. Kahn, *Molecular Magnetism*; Wiley-VCH, New York, **1993**, p. 8.
[21] T. T. M. Palstra, M. L. Steigerwald, A. P. Ramirez, Y.-U. Kwon, S. M. Stuczynscki, L. F. Schneemeyer, J. V. Waszczak, J. Zaanen, *Phys. Rev. Lett.* **1993**, *71*, 1768.
[22] ADF2006.01; SCM: Theoretical Chemistry, Vrije Universiteit, Amsterdam, The Netherlands, http://www.scm.com; a) E. J. Baerends, D. E. Ellis, P. Ros, *Chem. Phys.* **1973**, *2*, 41; b) E. J. Baerends, P. Ros, *Int. J. Quantum Chem.* **1978**, *S12*, 169; c) P. H. Boerrigter, G. te Velde, E. J. Baerends, *Int. J. Quantum Chem.* **1988**, *33*, 87; d) G. te Velde, E. J. Baerends, *J. Comput. Phys.* **1992**, *99*, 84; e) C. Fonseca Guerra, J. G. Snijders, G. te Velde, E. J. Baerends, *Theor. Chem. Acc.* **1998**, *99*, 391; f) G. te Velde, F. M. Bickelhaupt, S. J. A. van Gisbergen, C. Fonseca Guerra, E. J. Baerends, J. G. Snijders, T. Ziegler, *J. Comput. Chem.* **2001**, *22*, 931.
[23] S. Vosko, L. Wilk, M. Nusair, *Can. J. Chem.* **1980**, *58*, 1200.
[24] a) A. D. Becke, *J. Chem. Phys.* **1886**, *84*, 4524; b) A. D. Becke, *Phys. Rev. A* **1988**, 3098.
[25] a) J. P. Perdew, *Phys. Rev. B* **1986**, *33*, 8822; b) J. P. Perdew, *Phys. Rev. B* **1986**, *34*, 7406.

Received: December 18, 2007
Published Online: February 11, 2008

